CHEUNG, Howard; WANG, Shengwei. Impact of Dynamics on the Accuracies of Different Experimental Data-Processing Methods for Steady-State Heat Transfer Rate Measurement. Journal of Thermal Science and Engineering Applications, 2018, 10.2.
Journal of Thermal Sciences and Engineering Applications

Impact of Dynamics on The Accuracies of Different Experimental Data Processing Methods for Steady-state Heat Transfer Rate Measurement

Howard Cheung
The Hong Kong Polytechnic University
Room ZS 824,
The Hong Kong Polytechnic University,
Hung Hom, Kownloon, Hong Kong
hcheun@polyu.edu.hk

Shengwei Wang[1]
The Hong Kong Polytechnic University
Room ZS 859,
The Hong Kong Polytechnic University,
Hung Hom, Kownloon, Hong Kong
shengwei.wang@polyu.edu.hk

KEYWORDS
heat transfer rate; dynamics; steady state; laboratory measurement; uncertainty

ABSTRACT

It is becoming often to measure steady-state heat transfer rate from thermal systems with variable speed and volume equipment and hence with fluctuating properties and mass flow rates. However, it is unclear if the conventional heat transfer rate measurement based on averages of temperature and pressure measurement are representative enough to represent the effect of system dynamics and measure their heat transfer rates accurately. This paper studied the issue by comparing its accuracy and uncertainty to that of alternative data processing methods with theoretically less systematic bias. The comparison was conducted with steady-state data from a variable-speed ductless heat pump system with occasional

[1] Prof. Shengwei Wang is a Chair Professor of Building Services Engineering in the Department of Building Services Engineering in the Hong Kong Polytechnic University.

fluctuation of refrigerant flow and properties. The results show that the accuracy improvement brought by one alternative method is statistically significant albeit small in magnitude, and the other method may reduce uncertainty of the heat transfer rate measurement in tests with large periodic changes of measured variables. Nonetheless, both alternative methods are about 100 times more computationally expensive than the conventional averaging method, and averages of temperature and pressure measurement are still appropriate when computational resources are limited.

INTRODUCTION

Steady-state heat transfer rates are often measured from experiments to define the performance of various thermal systems such as unitary air-conditioning equipment [1], air-cooled heat exchangers [2] and water-to-water heat exchangers [3]. The conventional measurement method involves averaging sensor readings such as temperature and pressure before any thermodynamic property calculation to minimize the number of slow thermodynamic property calculation steps. This simplifies the calculation to a level that is feasible for engineers to conduct manually. Engineering standards recommending the conventional method include ASME Performance Test Code (PTC) 30-1991 on the performance of air-cooled heat exchangers [2] and British Standard EN 328:2014 [4] on the performance of air coolers for refrigeration. The practice was also widely used in literature such as evaluating water-to-water heat pump performance [5], measuring chiller cooling capacity [6], measuring air conditioner heat transfer rates [7], calculating heat transfer coefficient [8, 9] and measuring humidity removal rate [10]. The simplification also increases the systematic bias of the analysis and reduces its accuracy because not all pressure and temperature values remain

constant throughout an operation. As thermodynamic property calculation becomes more convenient with software tools to automate the traditional table lookup method and the graphical method for thermodynamic property calculation [21], it is feasible to drop the simplification to increase its accuracy. However, the analysis always involves uncertainties such as uncertainties of sensor measurement and uncertainties of the testing environment, and it is unknown if the accuracy improvement is meaningful under these uncertainties. The assumption that sensor readings remain constant at steady state also fit conventional heat exchanger operation well. There was no need to study the effect of the simplification to the accuracy of the analysis.

With the emergence of variable-speed and variable-volume thermal systems such as variable speed compressors and variable air volume boxes, the issue becomes important. It is questionable if measurement averages used in the conventional method are representative of the system dynamics when new systems run at constantly changing speed and volume instead of constant values at steady state. There are studies which address this issue under specific conditions. ASHRAE Standard 37-2009 recommended measuring the heat transfer rates of heat pumps during unsteady defrost operation by integrating the time profile of measured air temperature differences, but the method may not be appropriate for steady-state operation because it cannot quantify the random uncertainty from the laboratory environment [1]. Buswell studied uncertainty due to transients by creating an empirical rule based on its air-to-water heat exchanger and an exponential time profile for the non-steady operation but the rule might not be applicable for other types of time profiles and heat exchangers [11].

To understand how the simplification affects the accuracy of heat transfer rate measurement, this paper compares the heat transfer rates and their uncertainties measured by three different data processing methods. The data processing methods are generated by different simplifications on the first law of thermodynamics, and all of them are generalized unlike the ones in ASHRAE Standard 37-2009 [1] and Buswell [11] that are designed for specific conditions. The first method, which is the conventional method, calculates the heat transfer rate from measurement averages of sensor readings. The second method calculates the heat transfer rate by averaging instantaneous heat transfer rates, and the last method calculates the heat transfer rate by integrating instantaneous heat transfer rates. The comparison is conducted with the refrigerant-side heat transfer rates of a refrigerant-to-air heat exchanger which operating conditions may change periodically.

EXPERIMENTAL SETUP AND EXTRATION OF STEADY-STATE TEST

The evaluation of the data processing methods is conducted with the refrigerant-side measurement data from a condenser of a 3.52kW air-to-air ductless heat pump (DHP) system that uses a variable-speed compressor, an electronic expansion valve (EEV) and refrigerant R410A [12]. The condenser was a fin-and-tube heat exchanger. Superheated refrigerant vapor entered the condenser from the compressor and dissipated heat to the condenser airflow to deliver heating to the indoor environment. To change the airflow across the condenser, a variable-speed fan was used to drive the condenser airflow. Since only the heat transfer rate of the condenser is considered in

this paper, only the specification and the instrumentation of the condenser are described in this section. Further details of the setup including the test conditions of the DHP are listed in Appendix A for reference. The specification of the condenser is shown in Table 1.

Table 1 Geometry of the condenser of the ductless heat pump system

Tube outer diameter	0.734cm
Tube pattern	Staggered
Tube length	20.288m
Number of tubes rows per section	2
Number of tubes per row per section	5
Fin thickness	0.1538mm
Fin spacing	1.1cm
Fin density	7.87 fins/cm
Fin material	Aluminum
Tube material	Copper

On the refrigerant side of the heat exchanger, the temperature and the gauge pressure of refrigerant at the inlet and outlet were measured by T-type thermocouples and pressure transducers. A one-time measurement of atmospheric pressure was obtained by a mercury barometer to convert the gauge pressure readings into the absolute pressure of the refrigerant. A Coriolis mass flow meter was installed at the refrigerant outlet to measure the mass flow rate. On the air side, 8 T-type thermocouples were used to measure the inlet air temperature and 9 T-type thermocouples were used to measure the outlet air temperature. Standard airflow measurement nozzles were connected to the air outlet to measure the airflow rate according to ASHRAE Standard 41.2-1987 [13]. 2 chilled mirror sensors were used to

measure the dewpoint temperature at the air inlet and outlet. The data were collected at 10-second intervals with no extra samples being taken for analysis within the 10-second intervals. A general schematic of the experimental setup around the condenser is shown in Fig. 1.

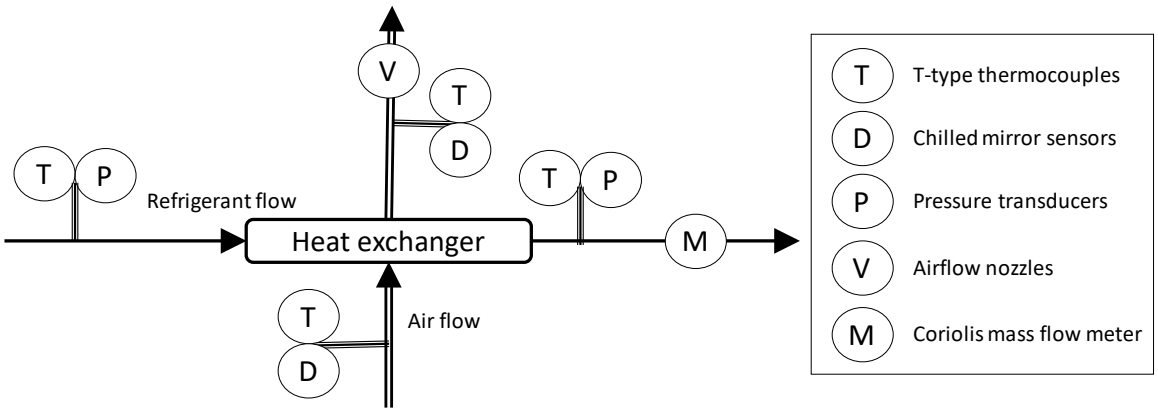

Fig. 1 Schematic of experimental setup around the DHP condenser

Besides the measurement around the heat exchanger, maximum and minimum compressor speed during the tests was also measured by attaching an accelerometer to the surface of the compressor of the DHP system.

To collect data of the heat exchanger under a variety of conditions, 28 different 20-minute experiments were conducted with data satisfying the criteria of steady state in Table 2.

Table 2 Criteria of steady state

Measurements	**Average rate of change within 20 minutes**
Refrigerant temperature at inlet and outlet of the heat exchanger	0.005 K/s
Refrigerant pressure at inlet and outlet of the heat exchanger	0.1 kPa/s
Refrigerant mass flow rate	0.006 kg/s^2

The steady-state data were verified to satisfy the requirement in ASHRAE Standard 37-2009 for valid refrigerant flow reading [1]. This ensured that the condenser outlet condition in the valid tests was subcooled liquid, and their thermodynamic properties could be defined from its temperature and pressure readings. The testing conditions of the condenser in these tests are shown in Table 3.

Table 3 Range of testing conditions of the condenser

Measured variable	Range of testing conditions
Refrigerant inlet temperature [°C]	52.7 to 87.1
Refrigerant inlet pressure [kPa]	2736 to 3540
Refrigerant mass flow rate [kg/s]	0.0114 to 0.0197
Air inlet temperature [°C]	17.7 to 24.5
Air inlet dewpoint [°C]	-3.7 to 5.9
Air volume flow rate [m^3/s]	0.0693 to 0.1083

Ideally, the controller of the DHP system should operate at constant compressor speed and EEV opening at steady state. However, real systems occasionally failed to do so because of control issues and their compressor speed and EEV opening changed periodically at steady state. The phenomenon also occurred in this study, and the ranges of fluctuation amplitude of the refrigerant temperature, pressure and mass flow rates in the 28 steady-state tests are shown in Table 4.

Table 4 Range of amplitude of changes of refrigerant conditions in tests of the condenser

Measured variable	Range of amplitude
Refrigerant inlet temperature [K]	0.3 to 7.1
Refrigerant inlet pressure [kPa]	6 to 394
Refrigerant mass flow rate [kg/s]	0.0001 to 0.0042

Table 4 shows that some tests in the data set behaved steadily while other tests were conducted with large changes of refrigerant properties and flow rate. An example of the fluctuation of refrigerant mass flow rates in one of the tests is illustrated in Fig. 2.

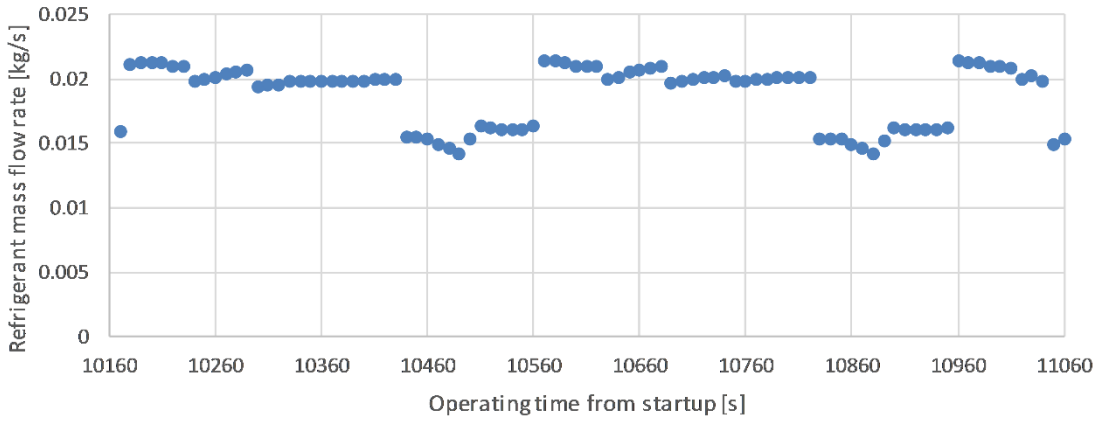

Fig. 2 Example plot of changes of refrigerant mass flow rates during the experiments when the compressor is changing its speed constantly

There are two kinds of uncertainties in experimental setups: systematic uncertainty and random uncertainty. The systematic standard uncertainties of the sensors, which are 68% confidence intervals of sensor readings, are listed in Table 5.

Table 5 Systematic standard uncertainties of sensors

Sensor	Standard uncertainty values
T-type thermocouples for refrigerant temperature	0.5K
Pressure transducers for refrigerant pressure	0.13% of full scale (6895kPa)
Coriolis mass flow meter for refrigerant mass flow rate	0.5% of measurement

Random uncertainty is a result of the random fluctuation in the testing environment and the sensor conditions, and it is calculated by statistical analysis of the

experimental result in this study. The statistical process may also capture any non-random fluctuation such as periodic changes in controls as random uncertainty.

DATA ANALYSIS

To study how the heat transfer rate measurement changes with data processing methods, three data processing methods were used to calculate the heat transfer rates in the DHP tests.

Data processing methods for heat transfer rate

Data processing method 1: Heat transfer rate from sample means of measurement data

This method is the conventional method used to measure heat transfer rate. Eq. (1) shows the measurement of steady-state heat transfer rate by sample means of measured variables, and Eq. (2) shows how a sample mean of measured variable from the i^{th} measurement device is calculated. By comparing Eq. (1) with the first law of thermodynamics in Eq. (3), it can be seen that Eq. (1) neglects the rate of change of heat exchanger internal energy and assumes that the temperature and pressure readings during the steady-state operation are the same. Hence their sample means can be used for heat transfer rate measurement.

$$\dot{Q}_{final,s1} = \bar{\dot{m}}\left(h(\overline{T_{in}}, \overline{P_{in}}) - h(\overline{T_{out}}, \overline{P_{out}})\right) \tag{1}$$

$$\overline{X_i} = \frac{\sum_{\ell}^{N} X_i(t_\ell)}{N} \tag{2}$$

$$\frac{d}{dt}E(t) = \dot{Q}(t) + \dot{m}_{outlet}(t)h(T_{outlet}(t), P_{outlet}(t)) - \dot{m}_{inlet}(t)h(T_{inlet}(t), P_{inlet}(t)) \tag{3}$$

While the method is appropriate for approximately constant temperature and pressure readings throughout the steady state, the assumption that the readings are constant may be violated if the readings are changing periodically with a large amplitude. This may lead to inaccurate measurement of steady-state heat transfer rates.

Data processing method 2: Heat transfer rate from sampling instantaneous heat transfer rate

The heat transfer rates can also be measured from the sample means of instantaneous heat transfer rate during steady-state experiments. The equations are shown in Eq. (4) and Eq. (5).

$$\dot{Q}_{final,s2} = \frac{\sum_{\ell}^{N} \dot{Q}_{inst}(t_\ell)}{N} \tag{4}$$

$$\dot{Q}_{inst}(t_\ell) = \dot{m}(t_\ell)\left(h\big(T_{in}(t_\ell), P_{in}(t_\ell)\big) - h\big(T_{out}(t_\ell), P_{out}(t_\ell)\big)\right) \tag{5}$$

This method does not assume that the temperature and pressure readings are constant. It only neglects the rates of change of heat exchanger throughout the steady-state operation. The relaxation of the assumption theoretically should reduce the systematic bias of the heat transfer rate measurement. However, the enthalpy values are calculated at each data acquisition time instant, and it takes more computation effort to process than processing method 1.

Data processing method 3: Sample mean of integrated heat transfer within a finite time period

Data processing method 2 still requires the instantaneous rate of change of heat exchanger internal energy to be negligible. However, the assumption may not be appropriate if the periodic changes of refrigerant properties and mass flow rates lead to periodic changes of the internal energy of the heat exchanger. This issue can be addressed by assuming that the change of internal energy is only negligible after a finite period of time as shown in Eq. (6) instead of assuming negligible instantaneous rate of change of internal energy.

$$\int_{t}^{t+\Delta t_f} E(t)dt = 0 \tag{6}$$

The resultant heat transfer rate can be calculated by Eq. (7).

$$\dot{Q}_{final,s3} = \frac{1}{M}\sum\nolimits_{i}^{M} \frac{1}{\Delta t_f}\left(\int_{t_i}^{t_i+\Delta t_f} \dot{Q}_{inst}(t_\ell)dt_\ell\right)_i \tag{7}$$

Since Eq. (7) cannot be integrated analytically with observations at discrete time intervals, it is approximated numerically by trapezoidal rule [17]. For experiments conducted with constant data acquisition frequency, the integration is done by Eq. (8).

$$\int_{t_1}^{t_1+\Delta t_f} \dot{Q}_{inst}(t_\ell)dt_\ell \approx \frac{1}{2}\dot{Q}_{inst}(t_1)\tau + \sum\nolimits_{i=2}^{V-1}\dot{Q}_{inst}(t_i)\,\tau + \frac{1}{2}\dot{Q}_{inst}(t_V)\tau \tag{8}$$

The computational speed of data processing method 3 is a little bit slower than that of data processing method 2 because data processing method 3 involves more

division operations for the integration time in Eq. (7) than that of data processing method 2.

Case studies of different data processing methods

To compare the accuracy and reliability of different data processing methods, three case studies are generated as shown in Table 6.

Table 6 Case studies by different data processing methods

Case study	Data processing methods
1	By sample means of measurement values (data processing method 1)
2	By sample means of instantaneous heat transfer rate (data processing method 2)
3	By sample means of integrated heat transfer (data processing method 3) with Δt_f at 1 minute

The uncertainty of measured heat transfer rate from these data processing methods follows ASME PTC 19.1-2013 [10] and can be generalized as Eq. (9).

$$u_{\dot{Q}_{final}} = \sqrt{b^2_{\dot{Q}_{final},sensor} + b^2_{\dot{Q}_{final},eos} + b^2_{\dot{Q}_{final},num} + a^2_{\dot{Q}_{final}}} \tag{9}$$

Equation (9) involves the systematic uncertainties of sensors, the systematic uncertainties of the equation of state for refrigerant properties, the systematic uncertainties of numerical methods and the random uncertainty due to sampling.

Propagation of the systematic uncertainty of sensor readings

The calculation computes the effect of the uncertainties of the sensors to the uncertainty of the heat transfer rates. All sensors in this study were calibrated with different calibration references. This implies that the thermocouples in the experiment were calibrated with different boiling water baths and iced water baths and the pressure transducers were calibrated with different standard pressure tanks. The propagation of their systematic uncertainties is calculated by Eq. (10).

$$b_{\dot{Q}_{final},sensor} = \sqrt{\sum_{i=1}^{O}\left[\sum_{\ell=1}^{N}\left\{\left(\frac{\partial \dot{Q}_{final}}{\partial X_i(t_\ell)} b_{X_i(t_\ell)}\right)^2 + \sum_{k=1,k\neq\ell}^{N}\left(\frac{\partial \dot{Q}_{final}}{\partial X_i(t_\ell)}\frac{\partial \dot{Q}_{final}}{\partial X_i(t_k)} b_{X_i(t_\ell)} b_{X_i(t_k)}\right)\right\}\right]} \quad (10)$$

Although Eq. (10) can be applied to heat transfer rate measurement of all data processing methods, the partial derivatives of heat transfer rates in Eq. (10) differ between data processing methods. Hence different data processing methods may yield different results from Eq. (10).

The first term in Eq. (10) propagates the systematic uncertainties by partial derivatives of heat transfer rate [14] and is commonly used to propagate sensor uncertainties to measurement results. The second term in Eq. (10) ensures that the systematic uncertainties of measurement by the same sensor at different time instants are not averaged by mistake. While taking measurement continuously by the same sensor at steady state reduces the random uncertainty, the repetition does not reduce the systematic uncertainty and the inappropriate reduction is prevented mathematically by adding the second term in Eq. (10).

Propagation of the systematic uncertainty of equation of state for refrigerant properties

To measure refrigerant-side heat transfer rate, enthalpy of the refrigerant is calculated from its equation of state (EOS). These EOS are semi-empirical equations created based on experimental observations of thermodynamic properties and physical laws behind refrigerant properties, and they estimate the thermodynamic properties with some uncertainties. By propagating the uncertainty of the EOS to the uncertainty of heat transfer rates, the effect of the uncertainty of the EOS to the heat transfer rate calculation can be understood.

While the literature of EOS provides the uncertainties of some thermodynamic properties such as density, they may not give the systematic uncertainties for enthalpy values [15, 16]. To estimate the uncertainty of enthalpy values, the relationship between specific enthalpy values and specific heat capacity of single-phase substance as shown in Eq. (11) is used.

$$\mathrm{h} = \int c_p(T, P)dT \tag{11}$$

The isobaric heat capacity of R410A from its EOS of mixtures is estimated with a relative systematic standard uncertainty at 0.5% [15]. The calculation of R410A properties in this paper depends on the EOS of pseudo-pure fluid of which specific capacity deviates from that of the EOS of mixtures by 0.1% [16]. Hence the uncertainty of the enthalpy of the EOS used in this paper can be estimated as 0.51% by sum of squares of the two deviations.

In data processing method 1, the enthalpy values are only calculated after averaging the measurement data within the 20-minute period in each test. Only two enthalpy calculation is involved and the propagation equation is given as Eq. (12).

$$b_{\dot{Q}_{final},eos,s1} = \sqrt{\begin{array}{l}\left(\frac{\partial \dot{Q}_{final}}{\partial h_{inlet}} b_{h_{inlet}}\right)^2 + \left(\frac{\partial \dot{Q}_{final}}{\partial h_{outlet}} b_{h_{outlet}}\right)^2 \\ +2\left(\frac{\partial \dot{Q}_{final}}{\partial h_{outlet}} \frac{\partial \dot{Q}_{final}}{\partial h_{inlet}} b_{h_{outlet}} b_{h_{inlet}}\right)\end{array}} \tag{12}$$

Data processing methods 2 and 3 calculate two enthalpy values per time instant. The systematic uncertainties of the enthalpy values all correlate with each other, and the resultant equation to calculate the propagation in the methods becomes Eq. (13).

$$\begin{aligned} & b_{\dot{Q}_{final},eos,s2} \text{ or } b_{\dot{Q}_{final},eos,s3} \\ &= \sqrt{\sum_{\ell=1}^{N} \left\{ \begin{array}{l} \left(\frac{\partial \dot{Q}_{final}}{\partial h_{inlet}(t_\ell)} b_{h_{inlet}(t_\ell)}\right)^2 + \left(\frac{\partial \dot{Q}_{final}}{\partial h_{outlet}(t_\ell)} b_{h_{outlet}(t_\ell)}\right)^2 \\ + \sum_{k=1,k\neq\ell}^{N} \left(\frac{\partial \dot{Q}_{final}}{\partial h_{inlet}(t_\ell)} \frac{\partial \dot{Q}_{final}}{\partial h_{inlet}(t_k)} b_{h_{inlet}(t_\ell)} b_{h_{inlet}(t_k)}\right) \\ + \sum_{k=1,k\neq\ell}^{N} \left(\frac{\partial \dot{Q}_{final}}{\partial h_{outlet}(t_\ell)} \frac{\partial \dot{Q}_{final}}{\partial h_{outlet}(t_k)} b_{h_{outlet}(t_\ell)} b_{h_{outlet}(t_k)}\right) \\ + \sum_{k=1}^{N} \left(\frac{\partial \dot{Q}_{final}}{\partial h_{inlet}(t_\ell)} \frac{\partial \dot{Q}_{final}}{\partial h_{outlet}(t_k)} b_{h_{inlet}(t_\ell)} b_{h_{outlet}(t_k)}\right) \\ + \sum_{k=1}^{N} \left(\frac{\partial \dot{Q}_{final}}{\partial h_{outlet}(t_\ell)} \frac{\partial \dot{Q}_{final}}{\partial h_{inlet}(t_k)} b_{h_{outlet}(t_\ell)} b_{h_{inlet}(t_k)}\right) \end{array} \right\}} \end{aligned} \tag{13}$$

Propagation of the systematic uncertainty of numerical methods

Numerical methods only approximates analytical solutions, and hence its results always carry systematic uncertainties. The systematic uncertainty of numerical methods is only relevant for data processing method 3 which uses a numerical trapezoidal rule.

The other two data processing methods do not involve numerical methods and their systematic uncertainties of numerical methods are always zero. In this paper, only the numerical uncertainty due to discretization is considered and the numerical uncertainties due to iteration and round off are assumed to be negligible. The calculation of the uncertainty is conducted by Richardson's extrapolation as shown in Eq. (14) and (15) [18].

$$b_{\dot{Q}_{final},s3,num} = \left| \frac{\dot{Q}_{final,s3} - \dot{Q}_{final,s3,long}}{\Gamma^{\lambda} - 1} \right| \tag{14}$$

$$\dot{Q}_{final,s3,long} = \frac{\Gamma}{M} \sum_{i}^{M} \frac{1}{\Delta t_f} \left(\frac{1}{2} \dot{Q}_{inst}(t_i)(\Gamma\tau) + \sum_{j=3,\text{j is odd}}^{V-1} \dot{Q}_{inst}(t_j)\,(\Gamma\tau) + \frac{1}{2} \dot{Q}_{inst}(t_V)(\Gamma\tau) \right)_i \tag{15}$$

Equation (14) and Eq. (15) approximate the uncertainty due to discretization by using heat transfer rate calculated from a coarser discretization on the time scale. The method calculates an estimate of the heat transfer rate with a coarser discretization ($\Gamma > 1$), and the difference between the original heat transfer rate and the heat transfer rate from coarser discretization is divided by a factor dependent on the order of accuracy of the trapezoidal method. In this paper, the ratio of discretization level is fixed at 2, and the order of accuracy of trapezoidal method is found to be 3 [17].

Propagation of the random uncertainty due to sampling

The random uncertainty due to sampling calculates the uncertainty of the random error source in the testing environment in the heat transfer rate calculation. For data processing method 1, the calculation begins with the calculation of sample

standard deviations of the data within the 20-minute steady-state operation. Sample standard deviation quantifies the random fluctuation of the data within the operation, and the equation to calculate the sample standard deviation of a variable X_i from the i[th] measurement device in the experiment is shown in Eq. (16).

$$s_{\overline{X_i}} = \frac{1}{M}\sqrt{\frac{\sum_{\ell}^{M}(X_i(t_\ell) - \overline{X}_i)^2}{M-1}} \tag{16}$$

To account for the dependence of random fluctuation between sensors, correlations between the time series of data are also considered in the random uncertainty calculation as shown in Eq. (17).

$$a_{\dot{Q}_{final},s1} = \sqrt{\sum_{i=1}^{O}\left[\left(\frac{\partial \dot{Q}_{final,s1}}{\partial \overline{X}_i} s_{\overline{X_i}}\right)^2 + \sum_{j=1,j\neq i}^{O}\left(r_{X_iX_j}\frac{\partial \dot{Q}_{final,s1}}{\partial \overline{X}_i}\frac{\partial \dot{Q}_{final,s1}}{\partial \overline{X}_j} s_{\overline{X_i}} s_{\overline{X_j}}\right)\right]} \tag{17}$$

$r_{X_iX_j}$ in Eq. (17) is the Pearson's correlation coefficient between the time-series data that quantifies the dependence between the i[th] and j[th] measurement device. It is calculated by Eq. (18).

$$r_{X_iX_j} = \frac{N\sum_{\ell}^{N} X_i(t_\ell)X_j(t_\ell) - \left(\sum_{\ell}^{N} X_i(t_\ell)\sum_{\ell}^{N} X_j(t_\ell)\right)}{\left[\left(N\sum_{\ell}^{N}(X_i(t_\ell))^2 - (\sum_{\ell}^{N} X_i(t_\ell))^2\right)\left(N\sum_{\ell}^{N}\left(X_j(t_\ell)\right)^2 - \left(\sum_{\ell}^{N} X_j(t_\ell)\right)^2\right)\right]} \tag{18}$$

For data processing method 2, since the averaging in Eq. (4) is only conducted on instantaneous heat transfer rates, the propagation of random uncertainty to the final heat transfer rate in Eq. (4) only considers the sample standard deviation of the instantaneous heat transfer rates. It is calculated by Eq. (19).

$$a_{\dot{Q}_{final},S2} = s_{\overline{\dot{Q}_{inst}}} = \frac{1}{M}\sqrt{\frac{\sum_{\ell}^{M}\left[\dot{Q}_{inst}(t_\ell) - \dot{Q}_{final,S2}\right]^2}{M-1}} \tag{19}$$

For data processing method 3, the random uncertainty of the steady-state heat transfer rate is calculated by the sample standard deviation of the average of the integrated heat transfer rates as shown in Eq. (20).

$$\begin{aligned} a_{\dot{Q}_{final},S3} &= s_{\overline{\left(\int_{t_i}^{t_i+\Delta t_f}\dot{Q}_{inst}(t_\ell)dt_\ell\right)/\Delta t_f}} \\ &= \frac{1}{M}\sqrt{\frac{\sum_{i}^{M}\left[\frac{1}{\Delta t_f}\left(\int_{t_i}^{t_i+\Delta t_f}\dot{Q}_{inst}(t_\ell)dt_\ell\right)_i - \dot{Q}_{final,S3}\right]^2}{M-1}} \end{aligned} \tag{20}$$

Tools used in data analysis

The computation of the calculation is programmed in Python 3.5.1 with refrigerant properties and property derivative calculated by software tools CoolProp version 5.1.2 [19, 20].

RESULTS AND DISCUSSION

Uncertainties of heat transfer rates

To compare the magnitude of uncertainties from different sources in all case studies, the relative expanded uncertainties of heat transfer rates, representing the 95% confidence interval of the heat transfer rates, are calculated according to Eq. (21), (22), (23), (24) and (25).

$$\text{Relative expanded uncertainty } = \vartheta_{0.95,M-1}\frac{u_{\dot{Q}_{final}}}{\dot{Q}_{final}} \tag{21}$$

$$\text{Relative systematic expanded uncertainty due to sensors} = \vartheta_{0.95,M-1}\frac{b_{\dot{Q}_{final},sensor}}{\dot{Q}_{final}} \tag{22}$$

$$\text{Relative systematic expanded uncertainty due to EOS} = \vartheta_{0.95,M-1}\frac{b_{\dot{Q}_{final},eos}}{\dot{Q}_{final}} \tag{23}$$

$$\text{Relative systematic expanded uncertainty due to numerical method} = \vartheta_{0.95,M-1}\frac{b_{\dot{Q}_{final},num}}{\dot{Q}_{final}} \tag{24}$$

$$\text{Relative random expanded uncertainty} = \vartheta_{0.95,M-1}\frac{a_{\dot{Q}_{final}}}{\dot{Q}_{final}} \tag{25}$$

To compare the uncertainties, their box plots in various cases are shown in Fig. 3, Fig. 4 and Fig. 5.

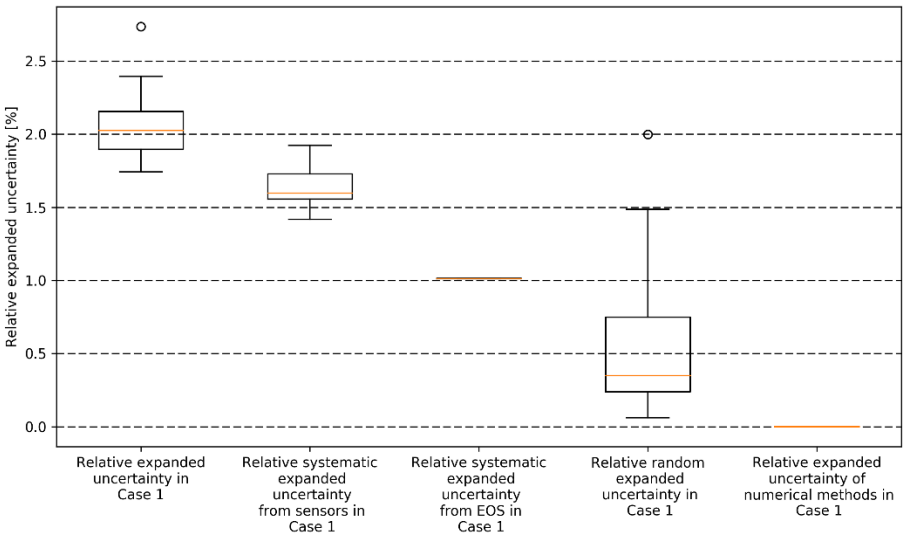

Fig. 3 Relative uncertainties of case 1 (data processing method 1)

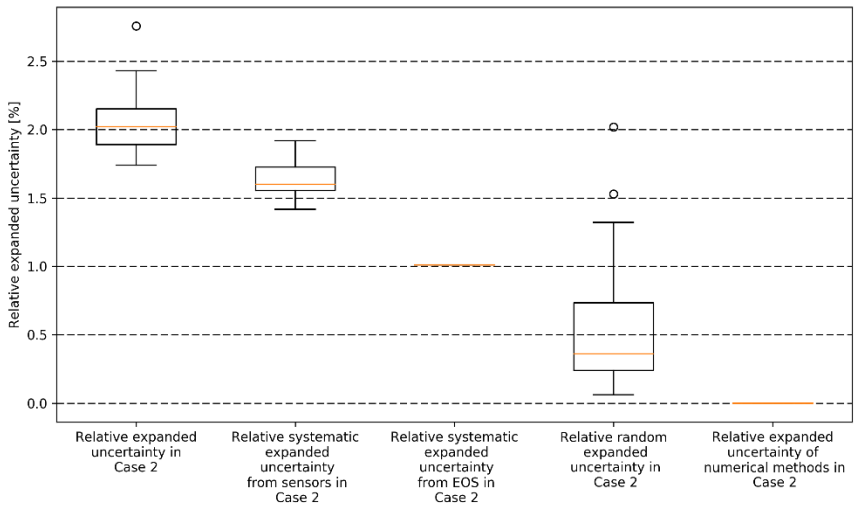

Fig. 4 Relative uncertainties of case 2 (data processing method 2)

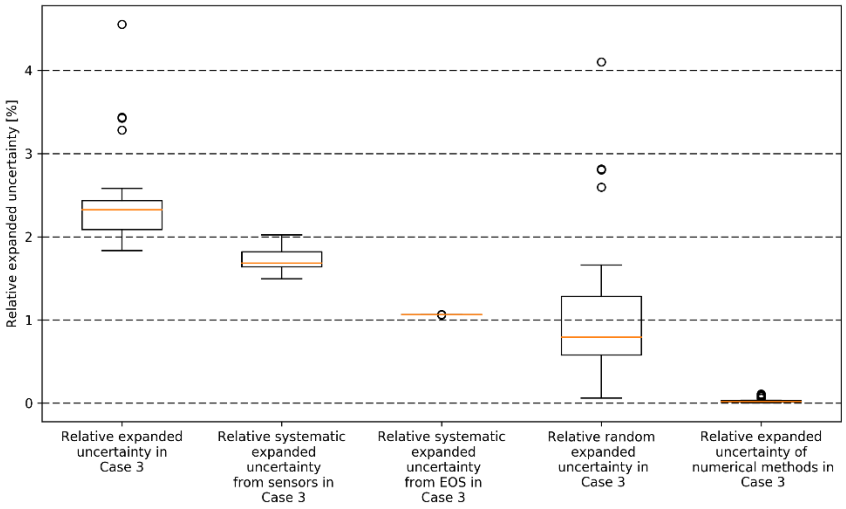

Fig. 5 Relative uncertainties of case 3 (data processing method 3 with Δt_f at 60 seconds)

Fig. 3 shows negligible difference between the uncertainties in cases 1 and 2. This implies that the relaxation of assumptions from data processing method 1 to method 2 has little effect on the magnitude of the uncertainty of the calculation.

However, the random uncertainties in case 3 are much larger than that of cases 1 and 2, which shows that the data processing method 3 is subjected to higher level of randomness than data processing methods 1 and 2. The reason lies in the number of samples in the cases. In cases 1 and 2, the number of samples equals to the number of time instants in a test which is 121. Case 3 needs data in 60 seconds to create 1 sample and has only 21 samples per test. This reduces the denominator of the sample standard deviation in Eq. (5) and increases its random uncertainty.

To study how the integration time interval affects the uncertainty of heat transfer rate, heat transfer rates were measured by processing method 3 with various integration time intervals at 20s, 40s, 60s, 100s, 120s, 200s, 240s, 300s, 400s and 600s. The calculation of the expanded uncertainties at 95% confidence level is shown in Eq. (26) and (27) [10].

$$\text{Expanded uncertainty of heat transfer rate} = \vartheta_{0.95,M-1} u_{\dot{Q}_{final}} \quad (26)$$

$$\text{Random expanded uncertainty} = \vartheta_{0.95,M-1} a_{\dot{Q}_{final}} \quad (27)$$

The results in four selected tests were plotted in Fig. 6, Fig. 7, Fig. 8 and Fig. 9 with the testing conditions listed in Table 7.

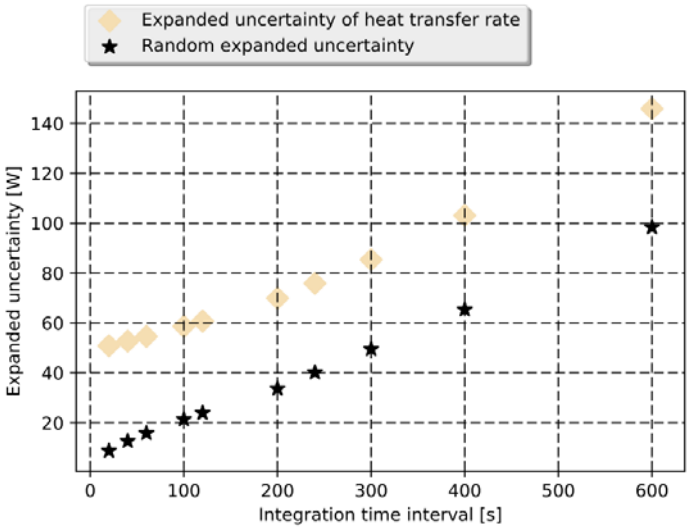

Fig. 6 Change of expanded uncertainty of heat transfer rate and random expanded uncertainty with integration time interval in experiment 1 in Table 7

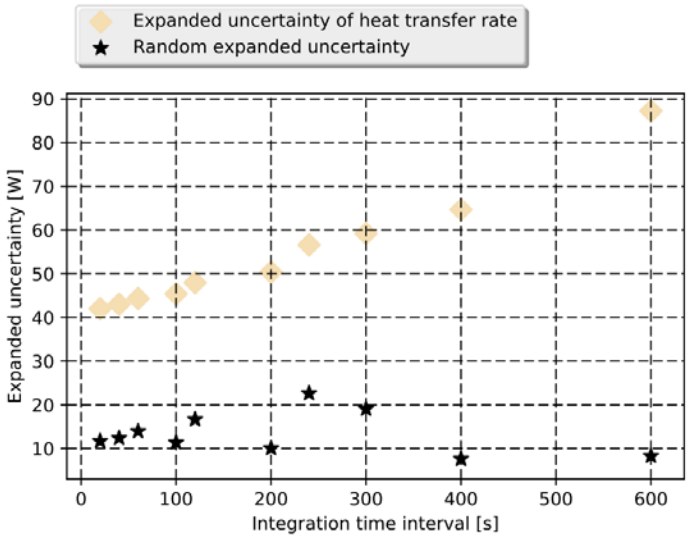

Fig. 7 Change of expanded uncertainty of heat transfer rate and random expanded uncertainty with integration time interval in experiment 2 in Table 7

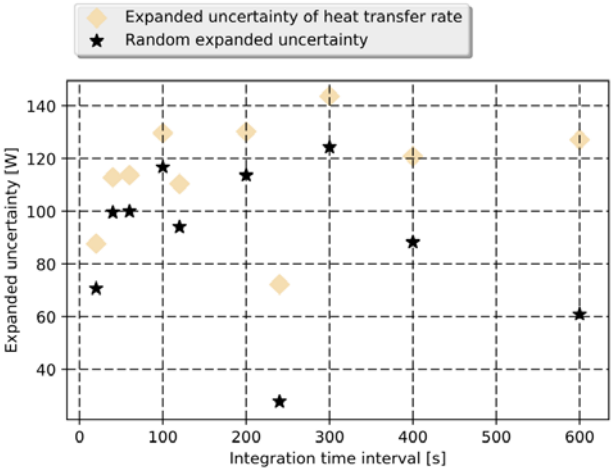

Fig. 8 Change of expanded uncertainty of heat transfer rate and random expanded uncertainty with integration time interval in experiment 3 in Table 7

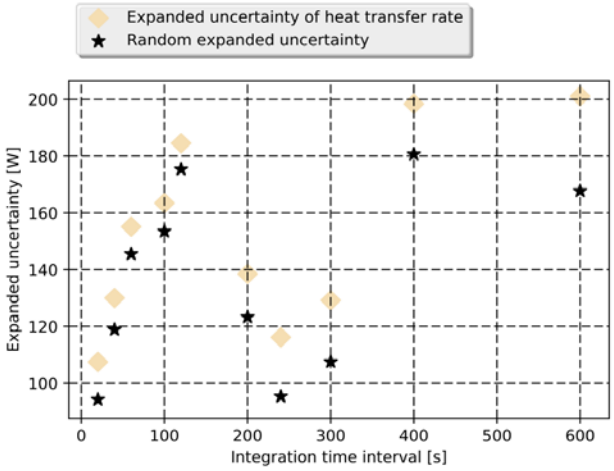

Fig. 9 Change of expanded uncertainty of heat transfer rate and random expanded uncertainty with integration time interval in experiment 4 in Table 7

Table 7 Testing conditions of experiments

Test	Indoor dry-bulb temperature [°C]	Outdoor dry-bulb temperature [°C]	Outdoor dewpoint [°C]	Compressor speed [Hz]	Indoor unit airflow [m^3/s]
Experiment 1	21.1	5.5	3.8	64.9	0.108

Experiment 2	21.2	8.3	-4.3	47.2 to 55.3	0.069
Experiment 3	21.2	1.7	-4.8	56.5 to 94.4	0.108
Experiment 4	21.2	1.7	-0.9	58.2 to 94.9	0.108

Fig. 6, Fig. 7, Fig. 8 and Fig. 9 show different behavior of uncertainty with integration time intervals for different tests. The test in Fig. 6 is conducted with constant compressor speed. Longer integration time interval only reduces the number of samples for heat transfer rate calculation and leads to higher random uncertainty. When the compressor speed starts to fluctuate, integration reduces the randomness due to periodic changes in the data, and the increase of random uncertainty by smaller sample size is compensated by the reduction of randomness. This is illustrated by the constant random uncertainty with integration time interval in Fig. 7. As the fluctuation of compressor speed becomes more significant, an appropriate integration time interval can reduce the effect of randomness to the measured heat transfer rate significantly and hence the random expanded uncertainty as illustrated by Fig. 8. Further investigation shows that the minimum random expanded uncertainty in Fig. 8 is 39.5W which is lower than the random standard uncertainty in processing methods 1 and 2 at 53.3W and 54.6W respectively, and hence processing method 3 can reduce random uncertainty due to periodic changes in compressor speed. Nevertheless, the method does not always reduce random uncertainty due to significant periodic fluctuation as illustrated by Fig. 9. The random standard uncertainties in data processing methods 1 and 2 are 71.3W and 71.7W respectively for the test in Fig. 9, and they are not

significantly smaller than the minimum random standard uncertainty in Fig. 9 which is 108.4W.

Accuracy of heat transfer rate measurement by data processing methods

To examine the improvement of the accuracy of heat transfer rate by different data processing methods, the maximum percentage difference between heat transfer rates from different data processing methods are calculated in Table 8.

Table 8 Maximum percentage difference of heat transfer rates between different data processing methods

Pair of data processing methods	Percentage difference
1 and 2	0.51%
2 and 3	0.12%
1 and 3	0.56%

Due to relaxation of assumptions, data processing method 3 should be more accurate than method 2, and method 2 should be more accurate than method 1. However, Table 8 also shows that there is not much accuracy improvement by using method 2 over method 1 and method 3 over method 2 with the maximum difference between heat transfer rates around 0.51% only. To examine whether the difference is offset by the uncertainty of the data processing methods, hypothesis testing was conducted on the difference of heat transfer rates between the data processing methods by calculating a z-statistic of the difference as shown in Eq. (28).

z-statistic of a test between case study i and j

$$= \left| \frac{\dot{Q}_{final(\text{case study i})} - \dot{Q}_{final(\text{case study j})}}{\sqrt{\begin{matrix} \sum_{k=1}^{O}\left(b_{X_k(\text{case study i})}^2 + b_{X_k(\text{case study j})}^2 - 2b_{X_k(\text{case study i})}b_{X_k(\text{case study j})}\right) \\ +b_{eos,(\text{case study i})}^2 + b_{eos,(\text{case study j})}^2 - 2b_{eos,(\text{case study i})}b_{eos,(\text{case study j})} \\ b_{num,(\text{case study i})}^2 + b_{num,(\text{case study j})}^2 - 2b_{num,(\text{case study i})}b_{num,(\text{case study j})} \\ +\sum_{k=1}^{O}\left(a_{X_k(\text{case study i})}^2 + a_{X_k(\text{case study j})}^2 - 2a_{X_k(\text{case study i})}a_{X_k(\text{case study j})}\right) \end{matrix}}} \right| \quad (28)$$

Equation (28) divides the difference between heat transfer rates with the standard uncertainty of the difference. The standard uncertainty of the difference is adjusted with the correlation of uncertainties of the same origin to avoid overestimation. If the z-statistic from Eq. (28) is larger than 2, the difference of the heat transfer rates between case studies is significant at 95% confidence level [10]. The calculation is conducted between results of different data processing methods, and the results are tabulated in Table 9.

Table 9 Percentages of tests with significantly different heat transfer rates at 95% confidence level

Pairs of data processing methods	Percentage of tests
1 and 2	100%
2 and 3	0%
1 and 3 (using case study 3)	60.7%

Table 9 shows that all heat transfer rates between data processing methods 1 and 2 are statistically different despite their small percentage difference in Table 8, while little significance can be found in other pairs of data processing methods. Since the assumptions in data processing method 2 are more relaxed than that of data

processing method 1, it can be said that data processing method 2 brings enough accuracy improvement over method 1 despite the uncertainties in the data processing methods.

To examine if the accuracy improvement brought by data processing method 2 increases with the dynamics of the data, the differences between heat transfer rates of data processing method 1 and 2 are plotted with the relative random expanded uncertainty of case study 1 in Fig. 10.

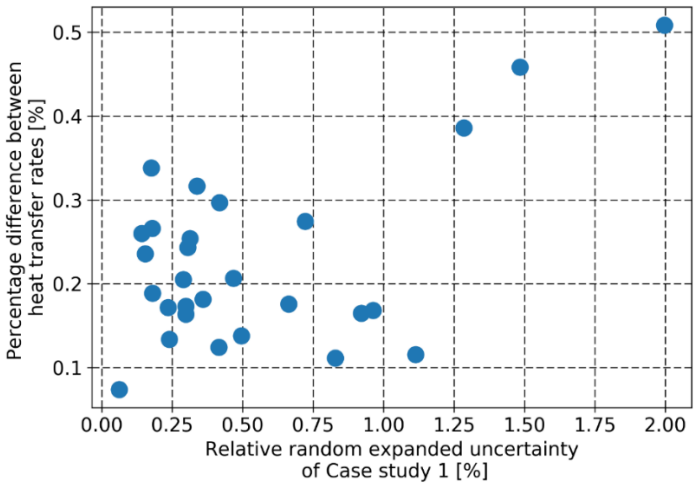

Fig. 10 Change of difference between heat transfer rates of data processing method 1 and 2 with relative random expanded uncertainty in case study 1

Percentage difference of heat transfer rate in Fig. 10 represents the improvement of accuracy by using data processing method 2 over data processing method 1, and relative random expanded uncertainty of case study 1 represents the degree of dynamics of data during steady state. The increase of percentage difference with random expanded uncertainty in Figure 6 shows that the degree of accuracy improvement increases with the dynamics of data, and data processing method 2 can

improve the accuracy of heat transfer rate measurement due to dynamics in measurement.

Complexity of data processing methods

To measure the computational complexity of the data processing methods, the computation speed of the data processing methods is measured in a 64-bit machine with four 3.4GHz central processing units and 4GB of memory. The results are tabulated in Table 10.

Table 10 Average computation speed of different data processing methods per test

Data processing method	Computational speed
1	0.0011 μs per test
2	0.1114 μs per test
3	0.1333 μs per test

Table 10 shows that data processing method 1 is the fastest because it only uses the equation of state twice per test. Its complexity is followed by data processing method 2 which calls the equation of state more often, and it takes 100 times longer to complete than data processing method 1. The most complex method is data processing method 3 which uses more arithmetic computation for its numerical integration.

CONCLUSIONS AND RECOMMENDATIONS FOR APPLICATIONS

In summary, the results show that the averaging of instantaneous heat transfer rate measurements improves the accuracy of heat transfer rate measurement from the conventional method by a small amount, and the accuracy improvement increases with the dynamics in measurement. Averages of integrated heat transfer rates may also help to reduce the random uncertainty in tests with large fluctuation of refrigerant

conditions if appropriate integration time interval is chosen. However, the alternative methods are more complex computationally and need more time to complete compared with the conventional method. Based on the analysis, the following recommendations on the data processing for heat transfer rate measurement are made:

1. Averaging instantaneous heat transfer rates is needed for obtaining the most accurate heat transfer rate.
2. The conventional data processing method for heat transfer rate measurement, i.e. averaging the sensor readings before thermodynamic property calculation, can be used if computational capacity of the control (monitoring) station is limited.
3. Averaging of integrated heat transfer rate is recommended to reduce the uncertainty of heat transfer rate caused by very large periodic changes of measured variables, and all possible integration time intervals should be attempted to find the proper interval for uncertainty reduction.

NOMENCLATURE

ASHRAE	American Society of Heating, Refrigerating and Air-Conditioning Engineers
ASME	American Society of Mechanical Engineers
a_X	Random standard uncertainty of variable X, unit varies
b_X	Systematic standard uncertainty of variable X, unit varies
c_p	Isobaric heat capacity, J/kg-K
Δt_f	Time interval for integration in processing method 3, seconds
E	Internal energy of heat exchanger, J
EEV	Electronic expansion valve
EOS	Equation of state
Γ	Ratio of time intervals of different discretization levels
h	Specific enthalpy, J/kg
λ	Order of accuracy of numerical methods
M	Number of samples in a processing method
N	Number of time instants within a steady-state test
O	Number of measurement sensors in the setup
P	Pressure, Pa
PTC	Performance Test Code
$\dot{Q}$	Heat transfer rate, W

$r_{X_i X_j}$	Pearson's correlation coefficient between variables X_i and X_j
$s_{\bar{X}}$	Sample standard deviation of variable X, unit varies
T	Temperature, K
t_ℓ	ℓ^{th} time instant, s
τ	Data acquisition time interval, s
$\vartheta_{0.95,\upsilon}$	Coverage factor according to Student t distribution at 95% confidence level and a degree of freedom υ
u	Standard uncertainty showing 68% confidence interval of the value, unit varies
V	Number of time instants within an integration time interval in processing method 3
X_i	Variable X of the i^{th} measurement device, unit varies

Accents

$\bar{}$ sample mean

Subscripts

eos	equation of state
final	steady-state test
inlet	inlet of condenser
long	longer integration time interval
inst	instantaneous

num	numerical method
$\dot{Q}_{final}$	heat transfer rate of the test
s1	processing method 1
s2	processing method 2
s3	processing method 3
sensor	sensor

REFERENCES

[1] ASHRAE. 2009. ANSI/ASHRAE Standard 37-2009 Methods of Testing for Rating Electrically Driven Unitary Air-Conditioning and Heat Pump Equipment. Atlanta, GA: American Society of Heating, Refrigerating and Air-Conditioning Engineers, Inc.

[2] ASME. 2016. ASME PTC 30-1991 (RA 2016) Air-Cooled Heat Exchanger. New York: American Society of Mechanical Engineers.

[3] BSI. 1999. BS EN 1148:1999 Heat Exchangers — Water-to-Water Heat Exchangers for District Heating — Test Procedures for Establishing the Performance Data. British Standards Institution.

[4] BSI. 2014. BS EN 328:2014 Heat Exchangers — Forced Convection Unit Air Coolers for Refrigeration — Test Procedures for Establishing the Performance. British Standards Institution.

[5] Payne, W. Vance, and Dennis L. O'Neal. 1999. "Multiphase Flow of Refrigerant 410A through Short Tube Orifices." ASHRAE Transactions 105: 66.

[6] Comstock, Matthew C. 1999. "Development of Analysis Tools for the Evaluation of Fault Detection and Diagnostics in Chillers." Master Dissertation, Purdue University.

[7] Shen, Bo. 2006. "Improvement and Validation of Unitary Air Conditioner and Heat Pump Simulation Models at off-Design Conditions." PhD Thesis, Purdue University.

[8] Stasiek, J., M.W. Collins, M. Ciofalo, and P.E. Chew. 1996. "Investigation of Flow and Heat Transfer in Corrugated passages—I. Experimental Results." International Journal of Heat and Mass Transfer 39 (1): 149–64. doi:10.1016/S0017-9310(96)85013-7.

[9] He, Xin, Jason A. Lustbader, Mehmet Arik, and Rajdeep Sharma. 2015. "Heat Transfer Characteristics of Impinging Steady and Synthetic Jets over Vertical Flat Surface." International Journal of Heat and Mass Transfer 80: 825–34. doi:10.1016/j.ijheatmasstransfer.2014.08.006.

[10] ASME. 2013. ASME PTC 19.1-2013 Test Uncertainty Performance Test Codes. New York: The American Society of Mechanical Engineers.

[11] Buswell, Richard A. 2001. "Uncertainty in the First Principle Model Based Condition Monitoring of HVAC Systems." PhD Thesis, Loughborough University.

[12] Cheung, Howard, and James E. Braun. 2014. "Performance Mapping for Variable-Speed Ductless Heat Pump Systems in Heating and Defrost Operation." HVAC&R Research 20 (5): 545–58. doi:10.1080/10789669.2014.917934.

[13] ASHRAE. 1987. ANSI/ASHRAE Standard 41.2-1987 (RA 1992) Standard Method for Airflow Measurement. Atlanta, GA: American Society of Heating, Refrigerating and Air-Conditioning Engineers, Inc.

[14] Kline, Stephen J., and F. A. McClintock. 1953. “Describing Uncertainties in Single-Sample Experiments.” Mechanical Engineering 75 (1): 3–8.

[15] Lemmon, Eric W., and Richard T. Jacobsen. 2004. “Equations of State for Mixtures of R-32, R-125, R-134a, R-143a, and R-152a.” Journal of Physical and Chemical Reference Data 33 (2): 593. doi:10.1063/1.1649997.

[16] Lemmon, E. W. 2003. “Pseudo-Pure Fluid Equations of State for the Refrigerant Blends R-410A, R-404A, R-507A, and R-407C.” International Journal of Thermophysics 24 (4): 991–1006. doi:10.1023/A:1025048800563.

[17] Chapra, Steven, and Raymond Canale. 2014. Numerical Methods for Engineers. 7 edition. New York, NY: McGraw-Hill Education.

[18] Roy, Christopher J., and William L. Oberkampf. 2011. “A Comprehensive Framework for Verification, Validation, and Uncertainty Quantification in Scientific Computing.” Computer Methods in Applied Mechanics and Engineering 200 (25–28): 2131–44. doi:10.1016/j.cma.2011.03.016.

[19] Bell, Ian H., Jorrit Wronski, Sylvain Quoilin, and Vincent Lemort. 2014. “Pure and Pseudo-Pure Fluid Thermophysical Property Evaluation and the Open-Source Thermophysical Property Library CoolProp.” Industrial & Engineering Chemistry Research 53 (6): 2498–2508. doi:10.1021/ie4033999.

[20] Thorade, Matthis, and Ali Saadat. 2013. “Partial Derivatives of Thermodynamic State Properties for Dynamic Simulation.” Environmental Earth Sciences 70 (8): 3497–3503. doi:10.1007/s12665-013-2394-z.

[21] ASHRAE. 2013. 2013 ASHRAE Handbook Fundamentals. Atlanta, GA: American Society of Heating, Refrigerating and Air-Conditioning Engineers, Inc.

APPENDIX A DESCRIPTION OF THE DUCTLESS HEAT PUMP SYSTEM

The performance testing of the ductless heat pump system was tested in psychrometric chambers to fix the temperature and humidity of air in the indoor room and outdoor room separately [12]. This controls the temperature and humidity of air entering the condenser and evaporator of the heat pump, and steady-state tests can be performed at fixed environmental conditions. The general schematic of the experimental setup is shown in Fig. 11.

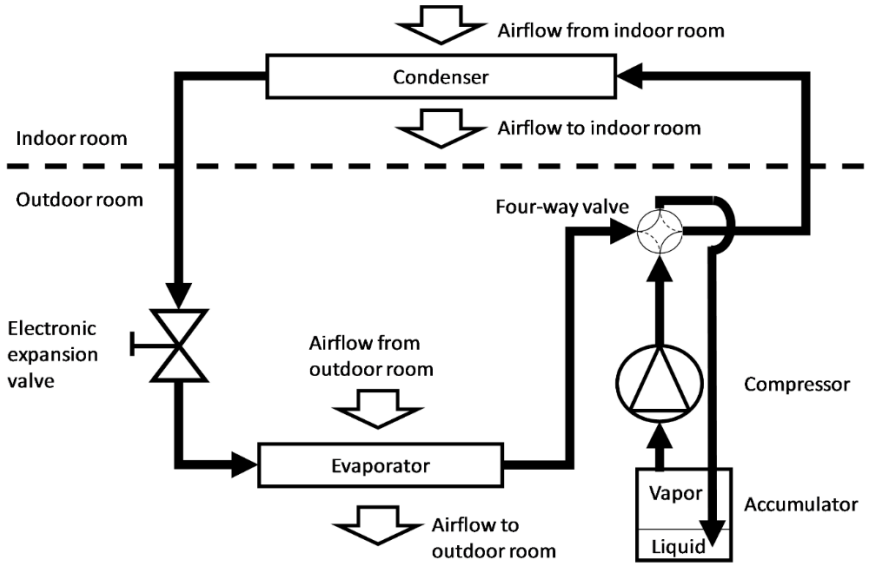

Fig. 11 Refrigerant flow in the ductless heat pump system in the psycrhometric chamber for its experiments of its heating operation

To achieve the range of testing conditions listed in Table 3, the temperature in the indoor and outdoor rooms of the psychrometric chamber was controlled separately to constant values in each test. The researcher instructed the controller to run the compressor and the fans at maximum speed, intermediate speed and low speed by the controller of the heat pump. A confidential algorithm in the heat pump would

determine final compressor speed, the condenser fan speed and the electronic expansion valve opening according to the user settings, and it might choose periodically changing speed and valve openings. The detailed testing conditions in the pscychrometric chamber was listed in Table 11 [12].

Table 11 Testing conditions in the psychrometric chamber and user settings of the heat pump

Indoor dry-blub temperature [°C]	Outdoor dry-blub temperature [°C]	Compressor speed [Hz]	Indoor unit airflow [m^3/s]
17.7 to 24.5	-19.6 to 16.8	48.0 to 94.8	0.0693 to 0.1083

Figure Captions List

Fig. 1 Schematic of experimental setup around the DHP condenser

Fig. 2 Example plot of changes of refrigerant mass flow rates during the experiments when the compressor is changing its speed constantly

Fig. 3 Relative uncertainties of case 1 (processing method 1)

Fig. 4 Relative uncertainties of case 2 (processing method 2)

Fig. 5 Relative uncertainties of case 3 (processing method 3 with Δt_f at 60 seconds)

Fig. 6 Change of expanded uncertainty of heat transfer rate and random expanded uncertainty with integration time interval in experiment 1 in Table 7

Fig. 7 Change of expanded uncertainty of heat transfer rate and random expanded uncertainty with integration time interval in experiment 2 in Table 7

Fig. 8 Change of expanded uncertainty of heat transfer rate and random expanded uncertainty with integration time interval in experiment 3 in Table 7

Fig. 9 Change of expanded uncertainty of heat transfer rate and random expanded uncertainty with integration time interval in experiment 4 in Table 7

Fig. 10 Change of difference between heat transfer rates of cases 1 and 2 with relative random expanded uncertainty in case study 1

Fig. 11 Refrigerant flow in the ductless heat pump system in the psycrhometric chamber for its experiments of its heating operation

Table Caption List

Table 1 Geometry of the condenser of the ductless heat pump system

Table 2 Criteria of steady state

Table 3 Range of testing conditions of the condenser

Table 4 Range of amplitude of changes of refrigerant conditions in tests of the condenser

Table 5 Systematic standard uncertainties of sensors

Table 6 Case studies by different data processing methods

Table 7 Testing conditions of experiments

Table 8 Maximum percentage difference of heat transfer rates between different data processing methods

Table 9 Percentages of tests with significantly different heat transfer rates at 95% confidence level

Table 10 Average computation speed of different data processing methods per test

Table 11 Testing conditions in the psychrometric chamber and user settings of the heat pump

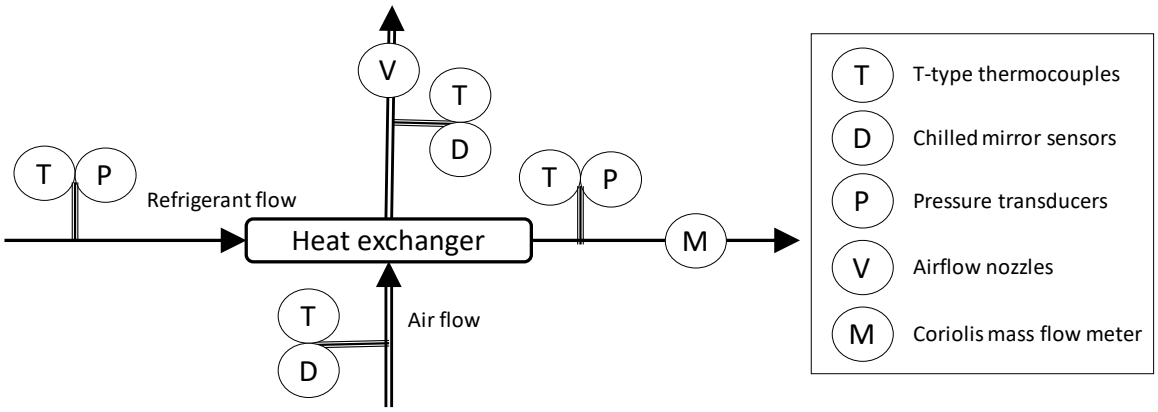

Fig. 1 Schematic of experimental setup around the DHP condenser

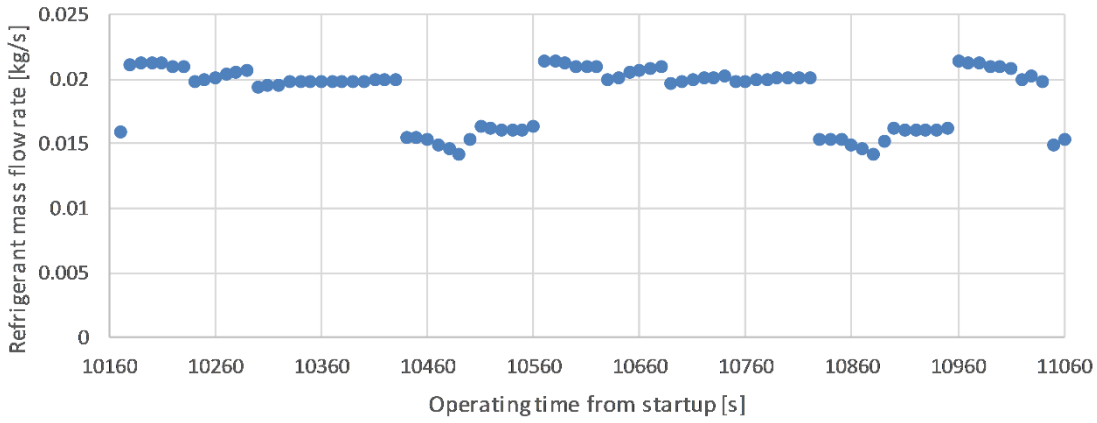

Fig. 2 Example plot of changes of refrigerant mass flow rates during the experiments when the compressor is changing its speed constantly

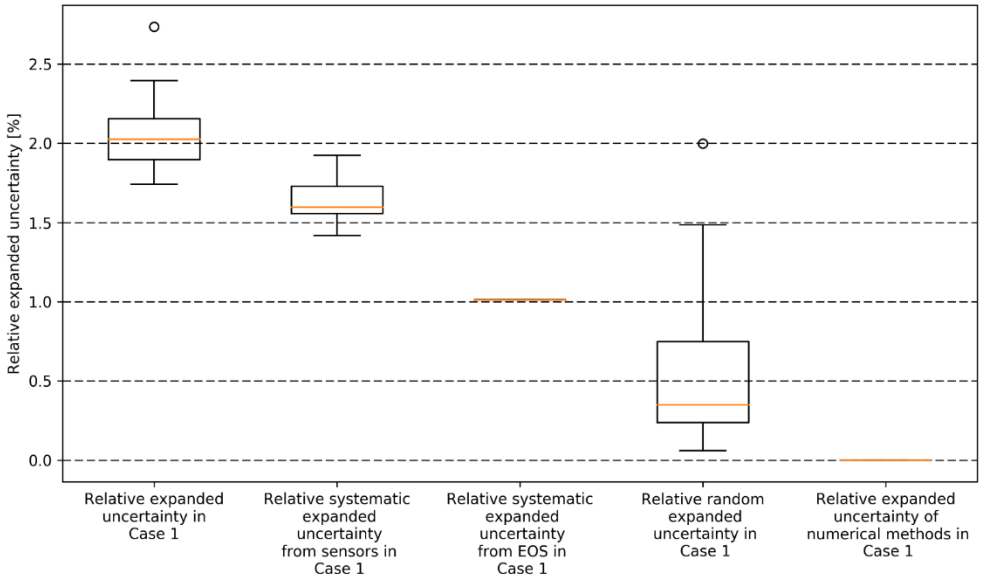

Fig. 3 Relative uncertainties of case 1 (data processing method 1)

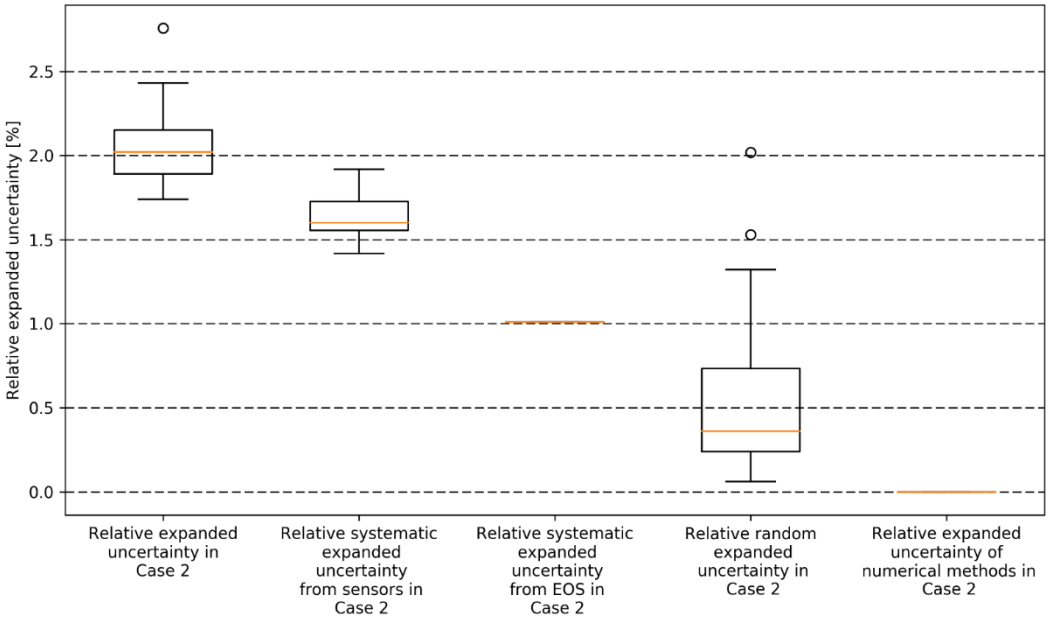

Fig. 4 Relative uncertainties of case 2 (data processing method 2)

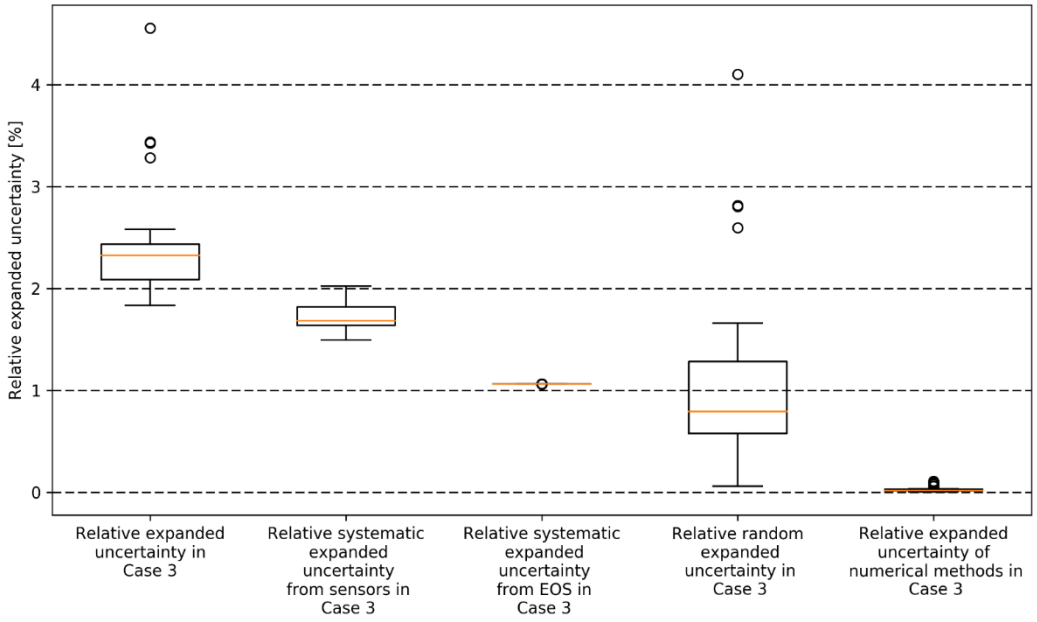

Fig. 5 Relative uncertainties of case 3 (data processing method 3 with Δt_f at 60 seconds)

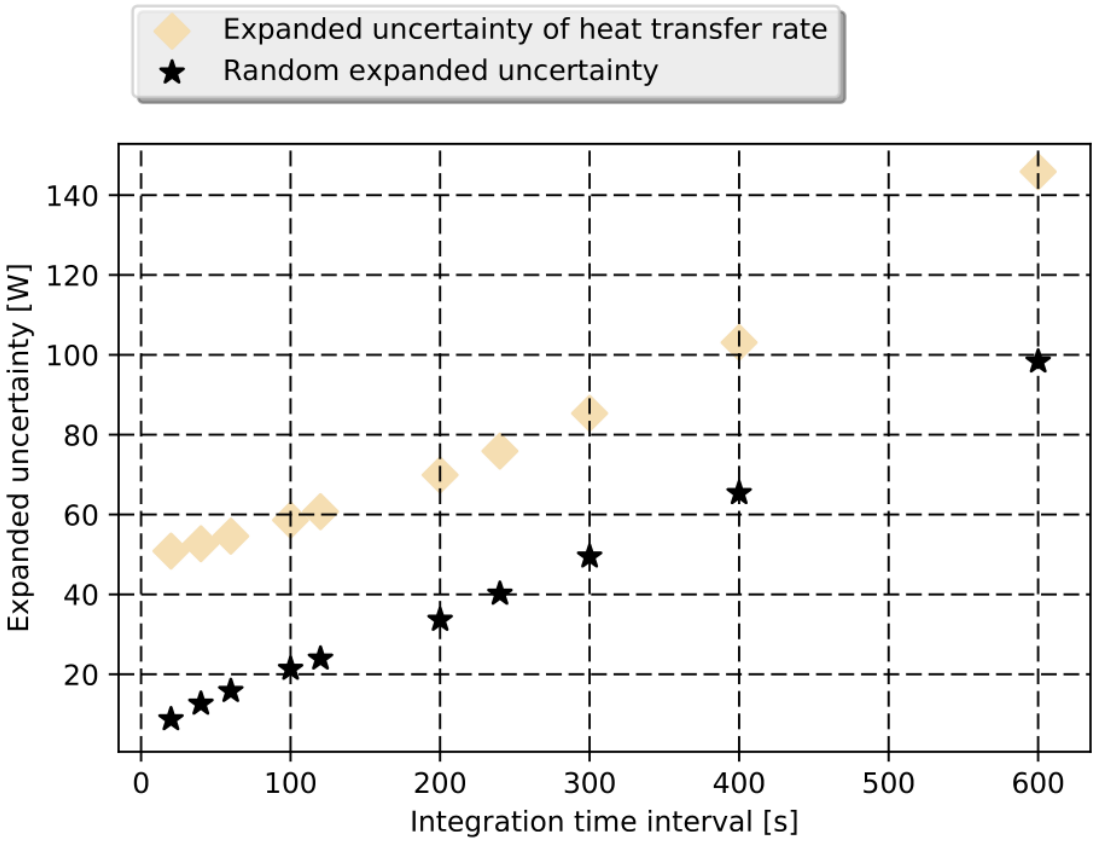

Fig. 6 Change of expanded uncertainty of heat transfer rate and random expanded uncertainty with integration time interval in experiment 1 in Table 7

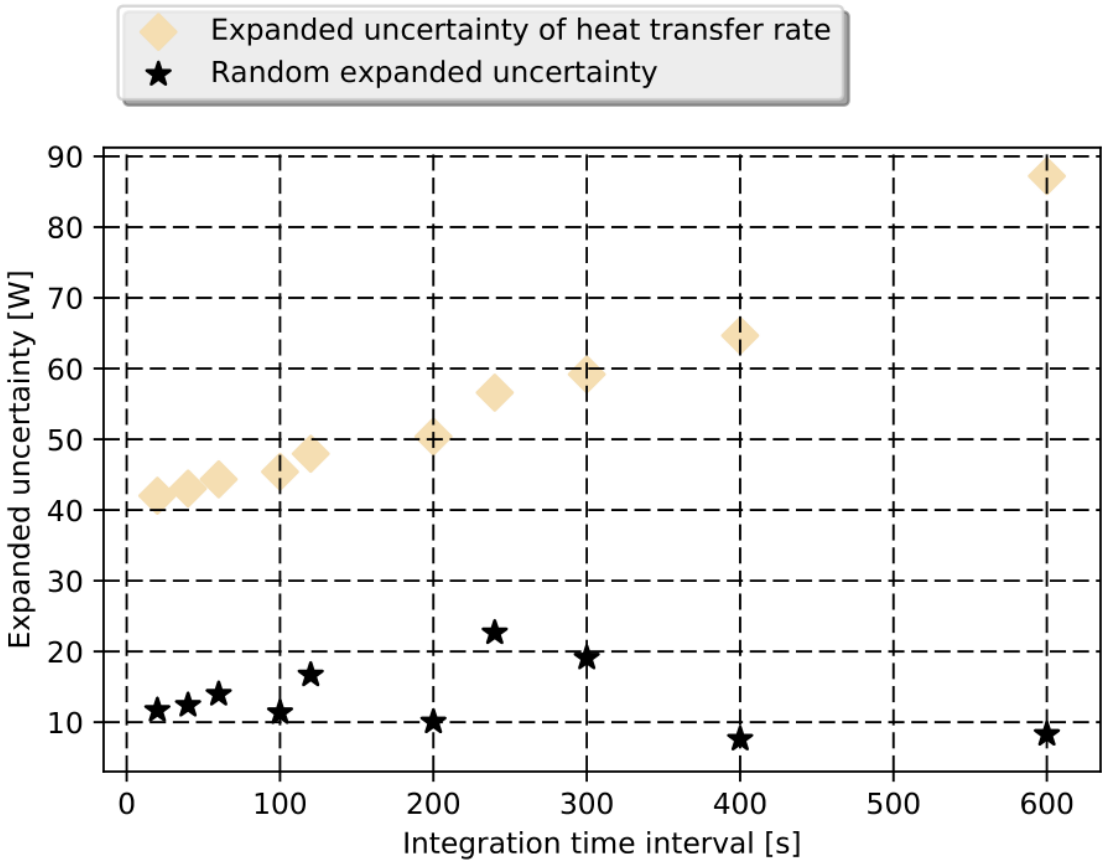

Fig. 7 Change of expanded uncertainty of heat transfer rate and random expanded uncertainty with integration time interval in experiment 2 in Table 7

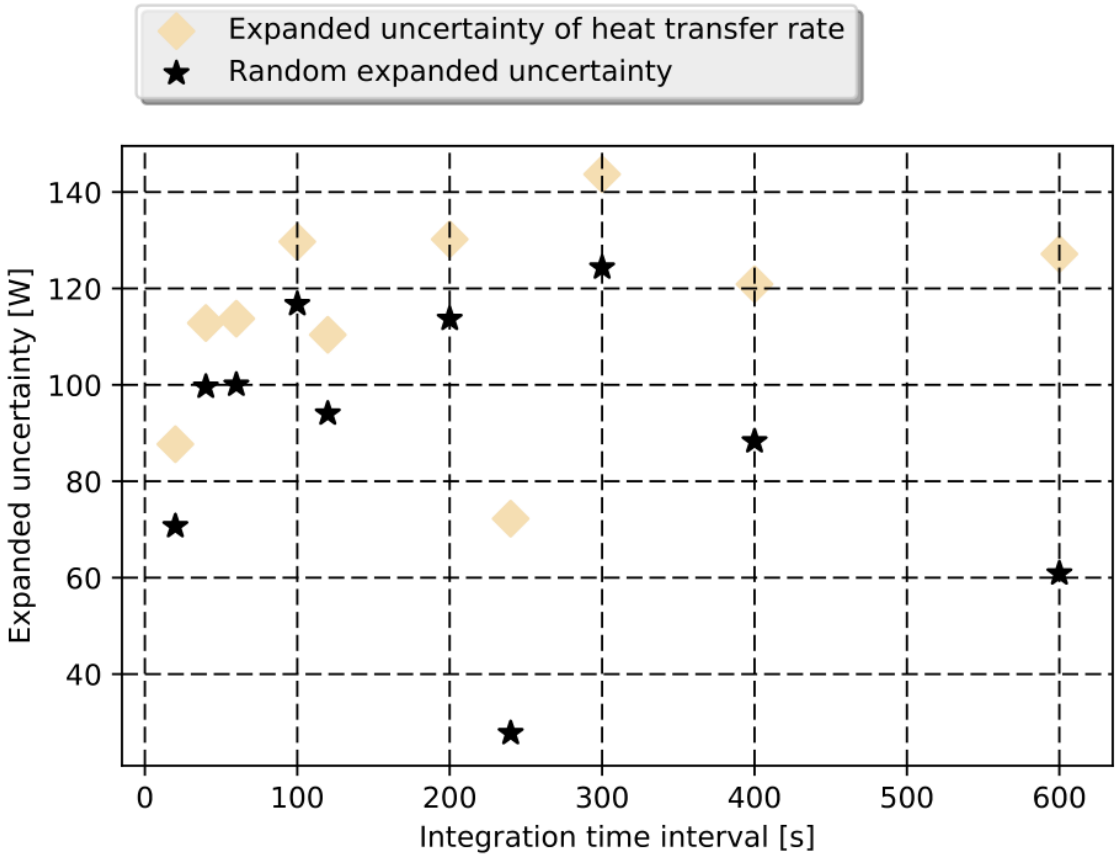

Fig. 8 Change of expanded uncertainty of heat transfer rate and random expanded uncertainty with integration time interval in experiment 3 in Table 7

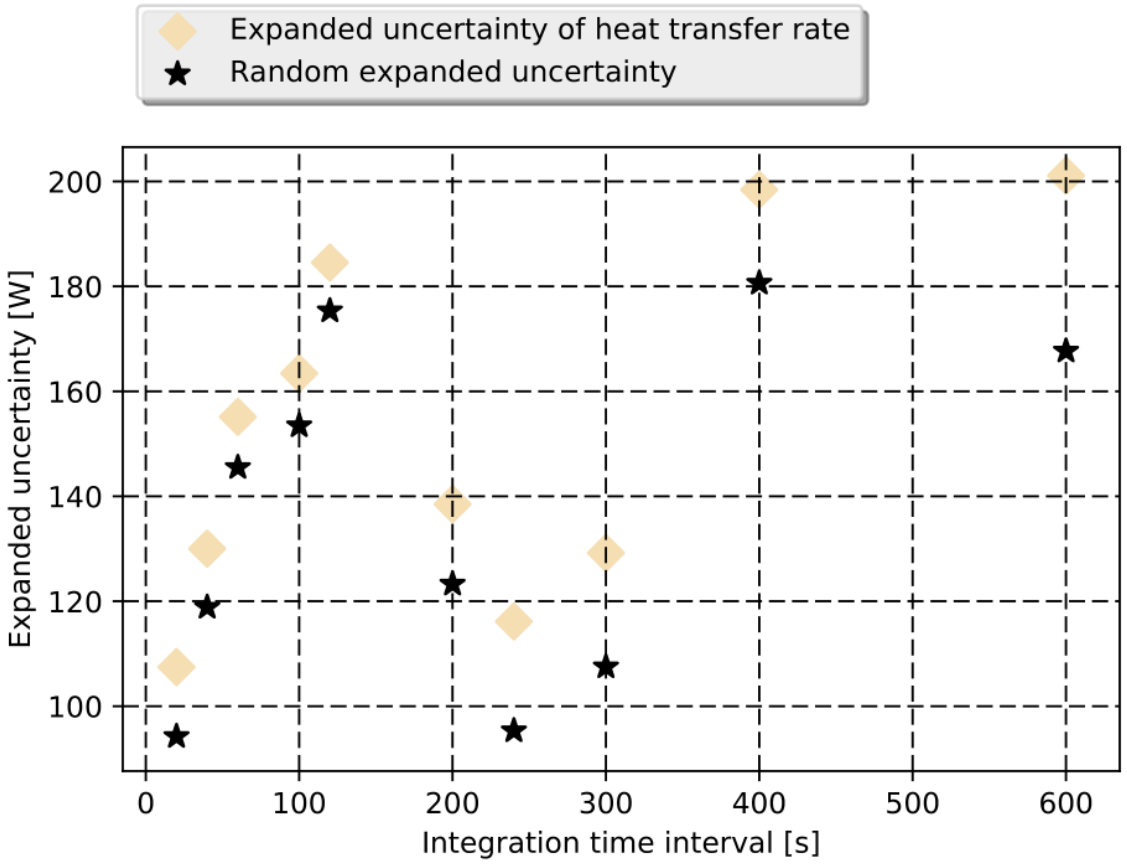

Fig. 9 Change of expanded uncertainty of heat transfer rate and random expanded uncertainty with integration time interval in experiment 4 in Table 7

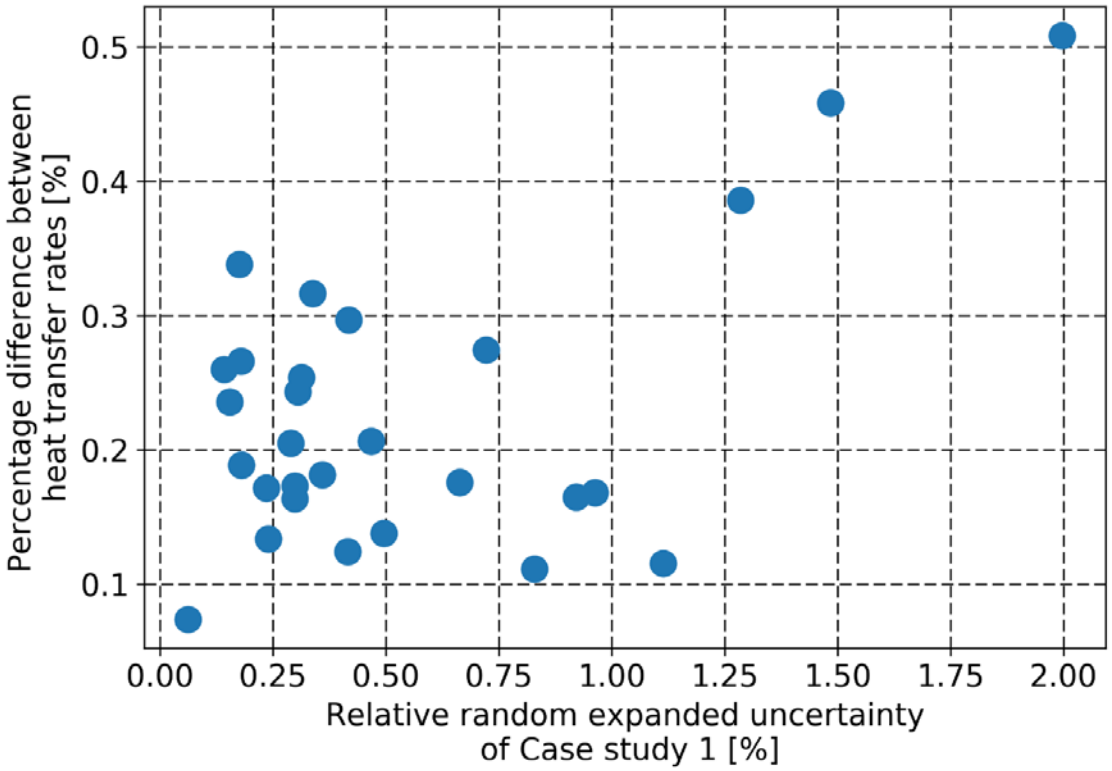

Fig. 10 Change of difference between heat transfer rates of processing method 1 and 2 with relative random expanded uncertainty in case study 1

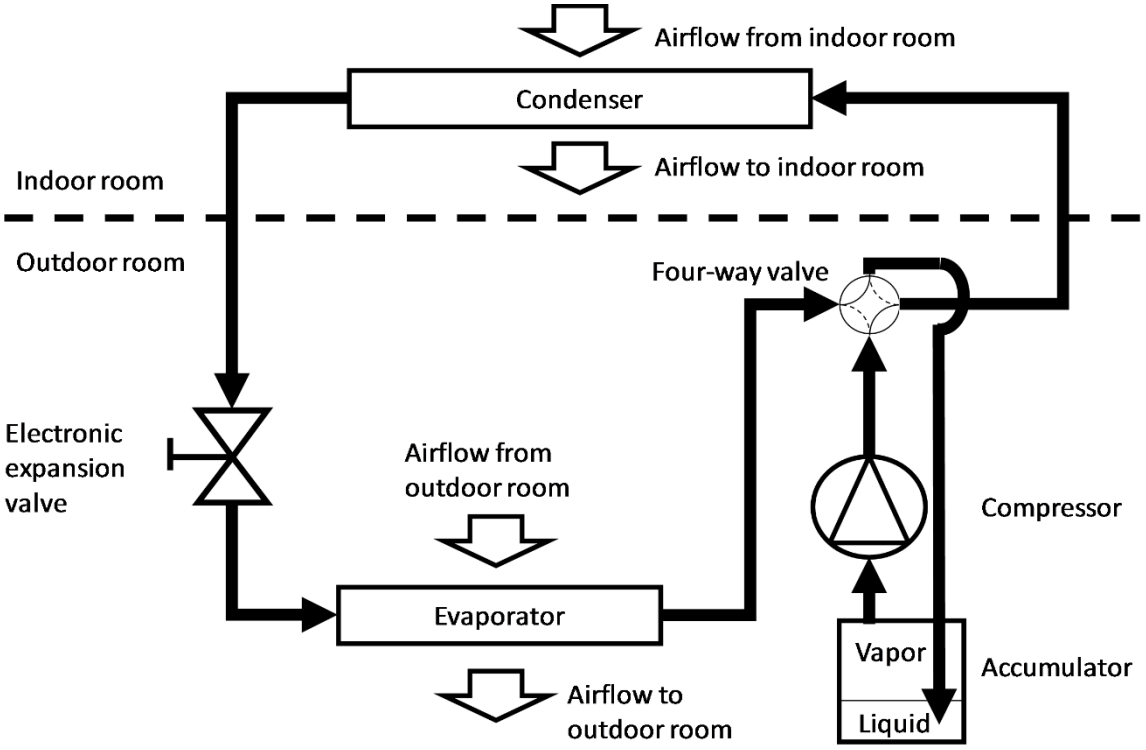

Fig. 11 Refrigerant flow in the ductless heat pump system in the psycrhometric chamber for its experiments of its heating operation

Table 1 Geometry of the condenser of the ductless heat pump system

Tube outer diameter	0.734cm
Tube pattern	Staggered
Tube length	20.288m
Number of tubes rows per section	2
Number of tubes per row per section	5
Fin thickness	0.1538mm
Fin spacing	1.1cm
Fin density	7.87 fins/cm
Fin material	Aluminum
Tube material	Copper

Table 2 Criteria of steady state

Measurements	**Average rate of change within 20 minutes**
Refrigerant temperature at inlet and outlet of the heat exchanger	0.005 K/s
Refrigerant pressure at inlet and outlet of the heat exchanger	0.1 kPa/s
Refrigerant mass flow rate	0.006 kg/s^2

Table 3 Range of testing conditions of the condenser

Measured variable	Range of testing conditions
Refrigerant inlet temperature [°C]	52.7 to 87.1
Refrigerant inlet pressure [kPa]	2736 to 3540
Refrigerant mass flow rate [kg/s]	0.0114 to 0.0197
Air inlet temperature [°C]	17.7 to 24.5
Air inlet dewpoint [°C]	-3.7 to 5.9
Air volume flow rate [m^3/s]	0.0693 to 0.1083

Table 4 Range of amplitude of changes of refrigerant conditions in tests of the condenser

Measured variable	Range of amplitude
Refrigerant inlet temperature [K]	0.3 to 7.1
Refrigerant inlet pressure [kPa]	6 to 394
Refrigerant mass flow rate [kg/s]	0.0001 to 0.0042

Table 5 Systematic standard uncertainties of sensors

Sensor	Standard uncertainty values
T-type thermocouples for refrigerant temperature	0.5K
Pressure transducers for refrigerant pressure	0.13% of full scale (6895kPa)
Coriolis mass flow meter for refrigerant mass flow rate	0.5% of measurement

Table 6 Case studies by different data processing methods

Case study	Data processing methods
1	By sample means of measurement values (data processing method 1)
2	By sample means of instantaneous heat transfer rate (data processing method 2)
3	By sample means of integrated heat transfer (data processing method 3) with Δt_f at 1 minute

Table 7 Testing conditions of experiments

Test	Indoor dry-bulb temperature [°C]	Outdoor dry-bulb temperature [°C]	Outdoor dewpoint [°C]	Compressor speed [Hz]	Indoor unit airflow [m^3/s]
Experiment 1	21.1	5.5	3.8	64.9	0.108
Experiment 2	21.2	8.3	-4.3	47.2 to 55.3	0.069
Experiment 3	21.2	1.7	-4.8	56.5 to 94.4	0.108
Experiment 4	21.2	1.7	-0.9	58.2 to 94.9	0.108

Table 8 Maximum percentage difference of heat transfer rates between different data processing methods

Pair of data processing methods	Percentage difference
1 and 2	0.51%
2 and 3	0.12%
1 and 3	0.56%

Table 9 Percentages of tests with significantly different heat transfer rates at 95% confidence level

Pairs of data processing methods	Percentage of tests
1 and 2	100%
2 and 3	0%
1 and 3 (using case study 3)	60.7%

Table 10 Average computation speed of different data processing methods per test

Data processing method	Computational speed
1	0.0011 μs per test
2	0.1114 μs per test
3	0.1333 μs per test

Table 11 Testing conditions in the psychrometric chamber and user settings of the heat pump

Indoor dry-blub temperature [°C]	Outdoor dry-blub temperature [°C]	Compressor speed [Hz]	Indoor unit airflow [m^3/s]
17.7 to 24.5	-19.6 to 16.8	48.0 to 94.8	0.0693 to 0.1083